Journal of the Serbian Chemical Society
JSCS@tmf.bg.ac.rs • www.shd.org.rs/JSCS
J. Serb. Chem. Soc. *89* (6) 857–875 (2024)
JSCS–5760
Original scientific paper
Published 30 June 2024

Exploring the efficacy of natural compounds against SARS-CoV-2: A synergistic approach integrating molecular docking and dynamic simulation

NABILA AOUMEUR[1], MEBARKA OUASSAF[2], SALAH BELAIDI[2]*, NOUREDDINE TCHOUAR[1], LOFTI BOURAGAA[2], IMANE YAMARI[3], SAMIR CHTITA[3]** and LEENA SINHA[4]

[1]University of Sciences and Technologies of Oran (USTO), Laboratory of Process Engineering and Environment, BP 1503 Oran 31000, Algeria, [2]Biskra University, LMCE Laboratory, Department of Matter Sciences, Biskra, Algeria, [3]Hassan II University of Casablanca, Laboratory of Analytical and Molecular Chemistry, Casablanca, Morocco and [4]University of Lucknow, Department of Physics, 226007 Lucknow, India

(Received 4 January, revised 28 January, accepted 3 March 2024)

Abstract: The primary aim of the current investigation is to contribute to SARS-CoV-2 research by identifying potential lead compounds for clinical applications, with a specific focus on inhibitors targeting the main protease (M^{pro}). In this research, molecular docking analysis was conducted using the software molecular operating environmental (MOE) to evaluate the potency of bioactive compounds sourced from medicinal plants as inhibitors of SARS--CoV-2 M^{pro}. Among 118 natural compounds with anti-HIV characteristics, the top seven candidates (h3, h84, h85, h87, h90, h108 and h110), were identified based on their superior binding energies with comparison to the reference ligand N3. These selected compounds exhibited binding affinities of –33.996, –35.336, –32.615, –32.154, –33.452, –31.903 and –40.360 kJ mol^{-1}, respectively. To further refine our shortlist of potential candidates for human application, we examined the drug-likeness, and the pharmaceutical attributes of these compounds using the SwissADME web server. Among them, only two compounds, namely h85 and h87, demonstrated favorable pharmacological properties suitable for human administration. These two compounds were subsequently shortlisted for further investigation. To explore the conformational stability of ligands within the M^{pro} active site, we performed molecular dynamics (MD) simulations. These simulations showed reliable and steady trajectories, supported by analyses of root-mean-square-fluctuation (*RMSF*) and root--mean-square deviation (*RMSD*). These findings and favorable molecular properties as well as interaction profiles suggest that these two lead compounds

* Corresponding authors. E-mail: (*)s.belaidi@univ-biskra.dz; (**) samir.chtita@univh2c.ma
https://doi.org/10.2298/JSC240104021A

may be promising SARS-CoV-2 therapeutic candidates. They present exciting starting points for further drug design.

Keywords: SARS-CoV-2; natural compounds; molecular docking; ADMET properties; dynamic simulation.

INTRODUCTION

With human-to-human transmission, the corona-virus 2 (SARS-CoV-2), which originated in China, quickly spread over the world and impacted a greater population.[1] This novel corona-virus disease 2019 (COVID-19), is called severe respiratory syndrome corona-virus 2 (SARS-CoV-2), and was first identified in December 2019 in the city of Wuhan, Hubei Province of China. Its high reproductive capacity played a pivotal role in the ensuing pandemic, leading to a significant loss of human lives, as documented by Huang *et al.*[2–4]

The World Health Organization (WHO) declared this disease a global health problem on January 30, 2020 with absolute urgency, involving international bodies, due to its continued progression. COVID-19 has spread to 200 nations worldwide,[5] with the United States, India, Brazil, Colombia, Russia, Spain, the United Kingdom and France being the most affected countries.[6] The most recent update states that the corona-virus family is a wide group of viruses that may cause disease in both humans as well as animals. Humans can get respiratory infections from many corona-virus strains, which can range from common colds to more serious diseases.[7]

As a zoonotic virus, SARS-CoV-2 has the potential to spread from animals to humans in the future, serving as a warning and indicator for sensible COVID--19 control and prevention efforts.[8] From its spread, SARS-CoV-2 generated rapid genomic changes, stimulating viral type selection. The WHO defines a variation of concern (VOC) as a viral variety that has evolved to outcompete other variations and affect public health.[9,10]

The COVID-19 pandemic has accelerated antiviral treatment research and use to unprecedented levels. Many chronic viral illnesses including HIV and hepatitis C have been successfully treated with antivirals. However, their use to treat acute viral infections like COVID-19 is limited. Computational tools have enabled the rapid analysis and sharing of viral genomes in recent years and allow near--real-time monitoring of viral alterations.[11]

These computational tools can predict the virus's replicative fitness and adaptation to the human host.[9]

The chymotrypsin-like protease ($3CL^{pro}$), commonly referred to as the main proteases (M^{pro}) and one or more known papain-like proteases with its abbreviation (PL^{pro}) are the two primary viral proteases found in coronaviruses.

The main proteases, recognized as M^{pro} or 3CLpro, play a vital role in the viral replication process. Their function involves cleaving polyproteins at various sites, leading to the production of different functional proteins.[12]

These 3CLpro enzymes are indispensable for coronavirus (CoV) replication, especially in the case of the severe pandemic caused by SARS-CoV and SARS--CoV-2 in the 21st century. Consequently, these have been tested as targets that have promising power for the design and development of broad-spectrum technologies of anti-CoV19 medications.[13]Most efforts to produce novel SARS--CoV-2 3CLpro inhibitors are based on previously published SARSCoV $3CL^{pro}$ inhibitors due to the significant association between the 14 various kinds of $3CL^{pros}$ generated from coronaviruses, as shown by their phylogenetic links. Because it is a potential target for managing different CoVs by limiting viral multiplication and pathogenesis, $3CL^{pro}$ has attracted a lot of attention from both the academic and business realms. The development of new anti-CoV drugs continues to rely heavily on the separation of active molecules from natural products. The use of naturally occurring substances that have been extracted from plants to treat a wide range of illnesses has received attention.[14] Many molecules of diverse chemical structures, from medicinal plants, have been proven to contain antiviral activity. Indicating that plants constitute a vast and unexplored potential supply of antiviral medicines. There is an outstanding review study on antiviral drugs extracted from plants.[15] There have been findings from molecular docking simulation studies using natural products and well-known antiviral medications to find possible therapeutic agents against the non-structural proteins of SARS--CoV-2.[16,17]

Biothermodynamic studies have provided intriguing insights into the complex dynamics of SARS-CoV-2 interactions by revealing the dynamic interactions between viral components and host receptors in epidemiology and pathophysiology research.[18–20]

Key findings from biothermodynamic studies on the interaction between SARS and CoV-2 are as follows. First, compared to Bat-CoV spikes, the spike glycoprotein (S-glycoprotein) of SARS-CoV-2 has a stronger affinity for the human ACE-2 receptor.[19] Second, the gut microbial ecology can be disrupted by even moderate instances of SARS-CoV-2 infection, which can result in a less stable gut microbiota.[20]

Third, although the pathogenicity of more recent SARS-CoV-2 variants, such as BF.7 and BA.5.2, has not changed, they are more contagious.[21,22] Fourth, fevers between 311 and 312 K can increase neutralizing antibodies binding affinities to the spike protein, which may reduce SARS-CoV-2's ability to infect others. Finally, Omicron sublineage spike glycoproteins bind to the ACE2 receptor more strongly at colder temperatures, which raises the possibility of increased viral transmission in the fall and winter.[19,23]

Previously, a prototype thermodynamic equilibrium model was developed for determining the dose–response potential of a respiratory virus such as SARS--CoV-2.[19]

Our study focused on 118 naturally occurring substances that have antiviral characteristics and particularly target HIV-1 (anti-HIV1). We selected these chemicals based on their potential, which has been previously identified, and the pathophysiological symptoms of COVID-19 and HIV-1 were shown to be identical. We additionally identified antiviral drug databases to be a useful source of motivation,[24] as agents against the SARS-CoV-2 (M^{pro}) with significant roles in viral replication/transcription and host cell recognition. This is achieved through the application of MD simulations, complemented by the computational assessment of drug-like and ADMET (absorption, distribution, metabolism, excretion and toxicity) properties for the highest-ranking compounds.[25–30]

We anticipate that this investigation will offer a comprehensive understanding of the binding and interaction between antiviral agents and the SARS--CoV-2 main protease (M^{pro}).

MATERIAL AND METHODS

Ligand identification

This study assembled a dataset comprising 118 natural chemical inhibitors specific to HIV-1, drawing upon previous research findings as documented in the literature.[16,30] Detailed information is available in Supplementary material to this paper (Fig. S-1 and Table S-I).

Table S-II of the Supplementary material outlines the binding energies of the 118 different chemicals to the protein identified by the PDB ID 6LU7. Fig. S-1 visually represents the optimized 2D molecular structures. These structures were generated using HyperChem 8.03 software[31] after an initial of sketch Marvin software.[32] The optimization of antiviral natural product geometries commenced with molecular mechanics[33] utilizing the MM+ force field with *RMS* = 0.0041 kJ/Å.[34] In addition, the PM3 semi-empirical approach was applied for subsequent geometric re-optimization.

Molecular docking simulations

The 3D structure of M^{pro} protein bound with N3 inhibitor was taken from the PDB website: Protein Data Bank (http://www.rcsb.org) with the PDB (ID: 6LU7).[35] In addition, MOE software (MOE, version 2007.09)[36,37] is applied for re-docking of co-ligands with the target and also for docking the studied molecules with M^{pro} SARS-CoV-2 protein.

The initial step involves the preparation of two proteins. By removing water molecules, the N3 inhibitor and adding polar hydrogen atoms into the structural conformation, as outlined by (Chtita *et al.*, 2022).[16] Subsequently, ligands designated for docking undergo structural optimization, and hydrogen atoms are added. According to Chtita *et al*.,[16] the site of action is defined as the volume occupied by the co-crystallized ligands in the pocket of each target following a well-determined orientation.

At pH 7.0, the PDB incoherence was adjusted, and the protonation state was assigned using the structure preparation mode of the MOE software. Alignment of key residues involved in ligand binding, such as: His41, Cys145, Met49, Thr45, Asp187, Asp187, Phe140, Arg188, Asn142, Gln189, Met165, Glu166 and His172, is remarkably high (*RMSD* = 0.99 Å)

in the ligand/binding pockets of the main protease of the SARS-CoV-2 virus, as shown in Fig. 1. It is thought that they facilitate the substrate's grid opening to the active state.[38]

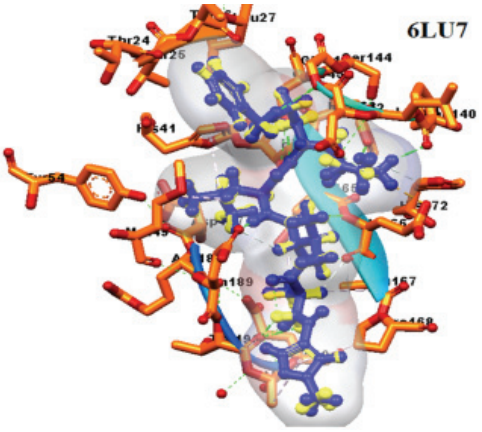

Fig 1. Binding -pocket with important residues of SARS-CoV-2virus M^{pro}(6LU7).

This study investigates molecular docking, examining the interactions between docked molecules and the key active sites. To determine which molecule exhibited the most effective interaction with the target, the results were based on the binding energy.[12,16]

In silico *pharmacokinetics analysis*

The development of novel drugs relies significantly on understanding their pharmacodynamic and pharmacokinetic properties. That interplays ADME and toxicology of chemicals within body, providing crucial insights into how a drug is processed and eliminated. Several methods, including Lipinski's Rule of Five (Ro5), were used to consider factors like Log *P* ligand molecular weight, and hydrogen bond donor and acceptor that serves as pivotal tools in predicting a compound's bioavailability.[39] Additionally, our investigation integrated Swiss ADME (http://www.swissadme.ch/) as a comprehensive platform to evaluate ADMET characteristics.[40]

Dynamics simulations

Molecular dynamics simulations of the two top-ranked ligand–protein complexes was made by using the Desmond module in Schrödinger software version 2021-3,[41] with the force fields: OPLS[42] to analyze and interpret the stability of the different interactions involved between the top-docked ligands and the protein in terms of binding affinity.

As a requirement for the limits, the system under study was delimited by an orthorhombic simulation box with 10 Å in three dimensions. The SPC is the solvation model water used in this simulation. The system was neutralized by adding 10 Na^+ and 6 Cl^-, and then 0.1 M NaCl was added as salt to modeling the physiology of the human body. The simulated system was optimized and reduced *via* the steepest descent minimization to eliminate steric collisions. The MDS was then run for 1ns at NVT equilibrium at 300 K, followed by NPT equilibrium by setting the experimental condition at 1.01325 bar and 300 K for the full simulation time (100 ns), to stabilize the system at the required conditions.

In the simulation, the first system, 6LU7-h85, comprised 43,652 atoms with 12,961 water molecules and had a net charge distribution of +10 from sodium ions and –6 from chloride ions. Conversely, the second system, 6LU7-h87, contained 43,643 atoms and 12,958

water molecules, and maintained the same charge distribution of +10 from sodium ions and –6 from chloride ions. Finally, many parameters were determined at the end of the simulation: we determine the mean square fluctuation/*RMSF* and the mean square deviation/*RMSD*, and all the protein–substrate interactions, with qualitative and quantitative aspects. The Desmond Structure program Schrödinger,[41] was used to create the graphics.

RESULTS AND DISCUSSION

Molecular docking investigation

This study focused on the protease Mpro, specifically targeting the (PDB ID 6LU7), as a prospective protein for inhibition of COVID-19. In the pursuit of proposing new inhibitors for 6LU7, it was important to investigate the inhibition mechanism employed by the most promising compound identified through comprehensive screening. Upon comparing the docked energies of all examined molecules, it becomes apparent that a significant proportion of ligands exhibit superior energy scores. This indicates that these compounds assume a more favorable docking pose compared to the reference ligand N3 (C35H48N6O8), whose interaction energy is listed in Table S-II as (–32.615 kJ/mol). To visualize the interactions of the reference ligand N3 within the active site of 6LU7 the MOE software was utilized. The analysis revealed that the reference ligand N3 when bound to the main protease then protease refers to an enzyme capable of degrading the peptide bonds connecting two amino acids present in proteins, so demonstrates inhibitory activity by making conventional hydrogen bonds with the amino acid Ser46 and one with Pro168 amino acid; π-alkyl interactions with Met49, His 163, His 41; and carbon-hydrogen bond with Gln189 of the enzyme (Fig. 2a).

Table I presents the results of molecular docking. Notably, the more negative binding energy values indicate that the complex has a good stability (Fig. 2a).The active site of the receptor enzyme comprises residues such as Met 49, Phe140, His41, Met165, Lue141, Glu166, His164, Gln192, His172, Leu27, Val42, Gln192, Thr190, Phe181, Asp187, Ala191, Cys145, Phe140, Arg188, Leu27 and Leu141.

The seven compounds h3, h84, h85, h87, h90, h108 and h110, which have the best binding score with the 6lu7 protein, are presented in (Fig. 2b).

Docked conformation of the compounds demonstrated that they are engaged in desirable interactions with the binding-pocket residues of the target protein, such as hydrophobic interactions, polar interactions, and hydrogen bonding. Hydrogen bonding or hydrogen bridge is an intermolecular or intramolecular force involving a hydrogen atom and an electronegative atom such as oxygen, nitrogen and fluorine. The intensity of a hydrogen bond is intermediate between that of a covalent bond and that of van der Waals forces.

The hydrogen bond binds with key residues inside the pocket are considered to be a determining factor in the average binding of the ligand with the active site of the receptor. The increased number of hydrogen bonds in the complex between

the ligand and protein may account for the higher binding affinity. The work of Imberty *et al*. indicates that interactions with distances between (2.5 and 3.1 Å), are considered strong interactions.[43] The hydrogen bond distances between the active site residues and the seven most favorable compounds range from 2.01 to 3.05 Å (Table I).

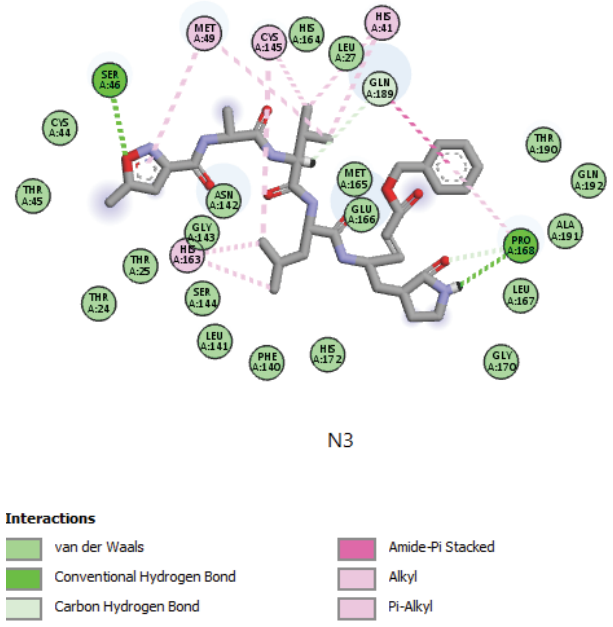

(a)

Ligand	Ligand-receptor interactions	Affinity, kJ/mol
h3	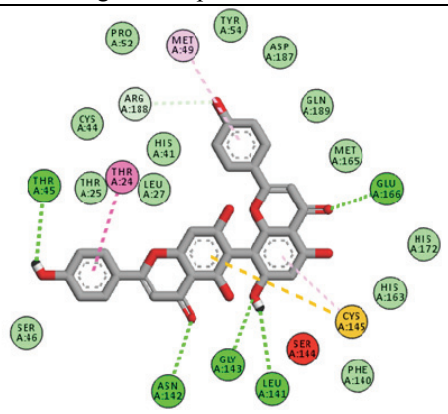	–33.996

(b)

Fig. 2. a) Diverse binding interactions of 6LU7 with N3 inhibitor; b) summary of docking interactions for M^{pro} SARS-CoV-2 protein.

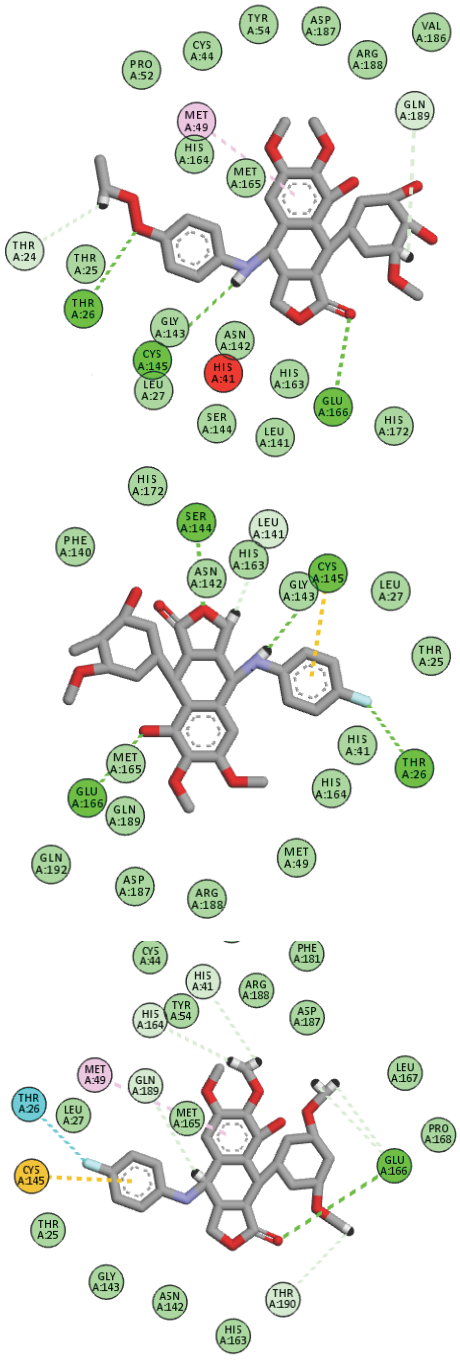

h84 –35.336

h85 –32.615

h87 –32.154

Fig. 2. Continued.

h90	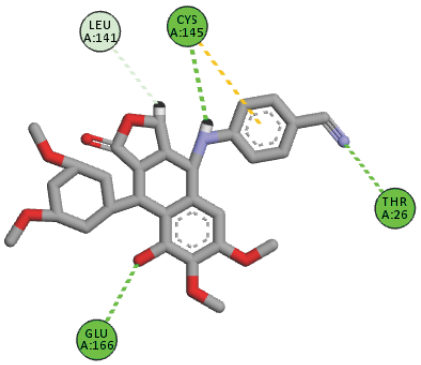	–33.452
h108	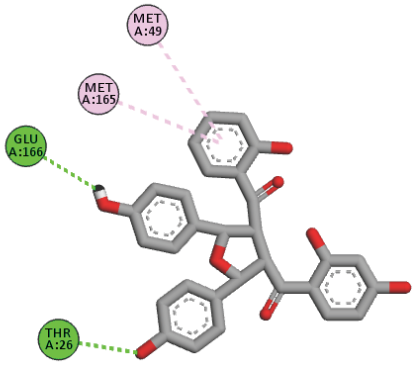	–31.903
h110	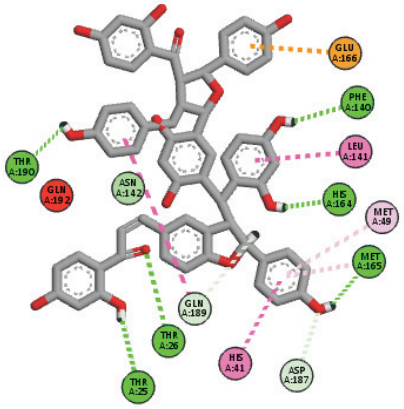	–40.360

Fig. 2. Continued.

Several antiviral medication studies have shown that inhibiting protease activity may cure several diseases caused by viruses. Hence, proteases emerge as potential targets for novel antiviral interventions. This inclination is grounded in the fundamental role that proteases assume during viral replication processes.[44]

TABLE I. Types of residue interactions and bond distances of the compounds examined with the residues of target protein 6LU7; strong interaction: 2.5 Å < *D* < 3.10 Å, and average interaction: 3.1 Å< *D* < 3.55 Å[43]

Compd.	Interaction type	Interaction residues of 6lu7	Distance, Å	Type of HB interaction
h3	H-Bond	Asn142, Glu166, Leu141, Gly143	3.05, 2.21, 2.24, 2.01, 2.36	Strong
	Pi-Anion	Cys 145	4.82	–
h84	H-Bond	Thr26, Glu166, Cys145	2.82, 2.98, 2.92	Strong
	Pi-Anion	Met 49	4.94	–
h85	H-Bond	Thr26, Ser144, Glu166, Cys 145	2.71, 2.38, 2.19, 2.62	Strong
	Pi-Anion	Cys 145	5.40	–
h87	H-Bond	Glu166	2.81	Strong
	Pi-Anion	Cys145	5.39	–
h90	H-Bond	Thr26, Glu166, Cys 145	2.37, 2.58, 2.19	Strong
	Pi-Anion	Cys 145	5.46	–
h108	H-Bond	Thr26, Glu166	2.11,2.30	Strong
h110	H-Bond	Thr26, Thr190, Thr25, Met165, His 164	2.90, 1.80, 2.85, 2.63, 2.72, 2.34	Strong
	Pi-Anion	Glu166	3.83	Average

To highlight potential drug candidates, an ADMET scan was done to examine the pharmacokinetics of the top-ranked ligands (h3, h84, h85, h87, h90, h108 and h110). An *in-silico* investigation allows for the exploration of pharmacokinetic parameters (ADMET). In medicinal chemistry, a key focus is the significance of high oral bioavailability in optimizing bioactive molecules for therapeutic purposes.

Drug-likeness and pharmacokinetic properties

Drug like-likeness or drug-like mainly evaluates the possibility for a molecule to become a drug in the future, orally based on its bioavailability. ADME predictions were conducted utilizing the freely accessible using the web-based software SwissADME,[40] on the following link: http://www.swissadme.ch. For drug-likeness studies, several rules were applied such as Lipinski's rule,[39] Veber's rule,[45] Ghose's rule,[46] Muegge's rule[47] and Egan's rule ,[48] these filters were recently tested in recent works.[49,50] The prediction, drug-likeness and ADME calculation results are shown in Tables II and III. According Table II, only the compounds h85, h87 and h90 exhibit a single violation according to Lipinski's rule. Meanwhile, three compounds (h3, h84 and h108 display more than one violation; however, they remain in the category of bioavailable ligands, but are less selective.[38]

The compound h110 displayed 4 violations (*HBD* > 5, *HBA* > 10, *MWt* > 500 Da, *TPSA* > 140 Å), therefore this ligand could have an oral bioavailability problem.

TABLE II. Results of applying Lipinski's Rule

Property	Bioactive compound						
	h3	h84	h85	h87	h90	h108	h110
MW (<500 Da)	538.46	583.63	539.59	525.57	532.58	512.51	1009.01
Log *P* (< 5)	0.25	1.70	2.59	2.40	1.37	1.32	1.02
H-bond donor (< 5)	6	2	1	1	1	5	11
H-bond acceptor (< 10)	10	11	9	9	9	8	15
Violations	3	3	1	1	1	2	4

TABLE III. Drug-likeness properties and ADME prediction of bioactive ligands

Drug-likeness property	Bioactive compound						
	h3	h84	h85	h87	h90	h108	h110
Lipinski	No	No	Yes	Yes	Yes	No	No
Veber (≤ 10 Rot, ≤ 140 *TPSA*)	No	Yes	Yes	Yes	Yes	No	No
TPSA / Å^2	181.80	134.34	95.65	95.66	119.44	144.52	275.13
Log (*S* / mol L^{-1})	–6.75	–5.55	–6.20	–5.84	–5.64	–6.19	–12.12
Bioavailability score	0.17	0.17	0.55	0.55	0.55	0.55	0.17
PAINS alert	0	0	0	0	0	0	0
GI	Low	Low	High	High	High	Low	Low
BBB permeability	No	No	No	No	No	No	No
Log *Kp*	–6.01	–7.15	–6.08	–6.30	–6.62	–5.93	–5.23
-Cyp1A2 inhibitor	No	No	Yes	Yes	Yes	Yes	No
-Cyp2C19 inhibitor	No	No	No	No	No	No	No
-Cyp2C9 inhibitor	No	No	No	No	No	Yes	No
-Cyp2D6 inhibitor	No	Yes	Yes	Yes	Yes	Yes	No
-Cyp3A4 inhibitor	No	No	No	No	No	No	No

The Veber filter stipulates that the *PSA*: polar surface area less than 140 Å^2 and the number of rotatable bonds (*nRotb* < 10 Å) for a ligand. On the contrary, compounds h3, h108 and h110 have *PSA* exceeding 140 Å^2, indicating a propensity for suboptimal bioavailability.

All of the compounds are well-suited for attaching to their targets because they contain less than 10 rotatable bonds, which helps them get away from the entropic penalty.

Three candidates showed less rule violations: Lipinski, Veber and Veber rules, those are the compounds h85, h87 and h90.Hence, based on Lipinski's "rule of five", Veber's rule and ADME characteristics, compounds h85, h87 and h90 may be the most suitable drug candidates amongst the originally chosen compounds.

Nevertheless, the RO5 test does not prove that the molecule has drug-like properties. The oral bioavailability of a drug, denoted *%F*, is the proportion of the administered dose which can reach the site of action. A score of 55 % is considered satisfactory, meaning it passes the five-fold test. With a score of 55 %, the substances h85, h87 and h90 demonstrated acceptable bioavailability. [38]

According to the results presented in Table III, we can say that the molecules h84, h8 and h90 have moderate solubility in aqueous solution, except h3, h85, h108 and h110, which have low solubility in the aqueous phase. According to the ADME properties, the absorption of the molecule in the intestine is described by the gastrointestinal (*GI*) factor, which is observed to be high; this explains that the compounds h85, h87 and h90 are strongly absorbed in the gastrointestinal system.

Certain parameters that can be exploited in computational calculation with a more or less reasonable degree of accuracy include penetration across the CNS: central nervous system or the BBB: the blood-brain barrier. It's noteworthy that all the compounds do not present any permeability through the BBB barrier.

Two molecules were found capable of passing ADME profiling for the study of toxicity among the seven molecules. using the Pro-Tox web server with reference to the Globally Harmonized System.[51]

The significant enzyme in the family of CYP: CYP3A4, is responsible for metabolism of half of all medications. Another enzyme in the family, CYP2C9, metabolizes several pharmaceuticals that are used in clinical settings, including the drug diclofenac and celecoxib.[52] The Table IV shows that the bioactive ligand h87 is a substrate for CYP2C9.

TABLE IV. Toxicity of bioactive compounds

Compound	Hepatotoxicity	Carcinogenicity	Mutagenicity	Cytotoxicity	LD_{50} / mg kg^{-1}
h3	No	No	No	No	2430
h84	No	No	No	No	3000
h85	No	No	No	Yes	500
h87	No	No	No	Yes	500
h90	No	No	Yes	No	500
h108	No	No	No	No	1500
h110	No	No	No	No	2000

Compounds h84, h85, h87, h90, and h108 in our study act as inhibitors for the CYP2D6 enzyme, which is crucial in metabolizing about 25 % of known pharmaceuticals, contributing to potential clinical issues. However, two compounds, h3 and h110, identified in Table IV, are non-inhibitors of CYP2D6.

The Boiled-Egg Plot, a feature available through SwissADME, is used to assess BBB barrier permeability and passive gastrointestinal absorption of the compounds under investigation. This graph juxtaposes the lipophilicity of a compound with its *TPSA* surface area.[40,53] Compounds located in the inner yellow region result in gastrointestinal absorption in the white region, are predicted to possess permeability across the blood-brain barrier. Conversely, compounds beyond the gray zone may have physicochemical properties less conductive to passive gastrointestinal absorption and blood–brain barrier penetration.

An influential participant in the natural elimination of various medications with diverse molecular structures, the permeability glycoprotein (*P-gp*) serves as a crucial protein transporter.[50] The chemicals that are expected to be pumped up from the brain or the gastrointestinal lumen as substrates of the P-glycoprotein (PGP+) are shown by the points colored by blue (h84, h85, h87 and h90). Points in red, such as molecules h3 and h108, are associated with P-glycoprotein non--substrates (PGP-).

Compounds h85, h87 and h90, positioned in the white region of the SwissADME Boiled-Egg Plot (Fig. 3), are expected to behave like small ligands, which have a high likelihood of gastrointestinal absorption. Conversely, compounds h3, h84 and h108, located in the grey region, are expected to have less--than-ideal brain permeability across the membrane CNS.[52]

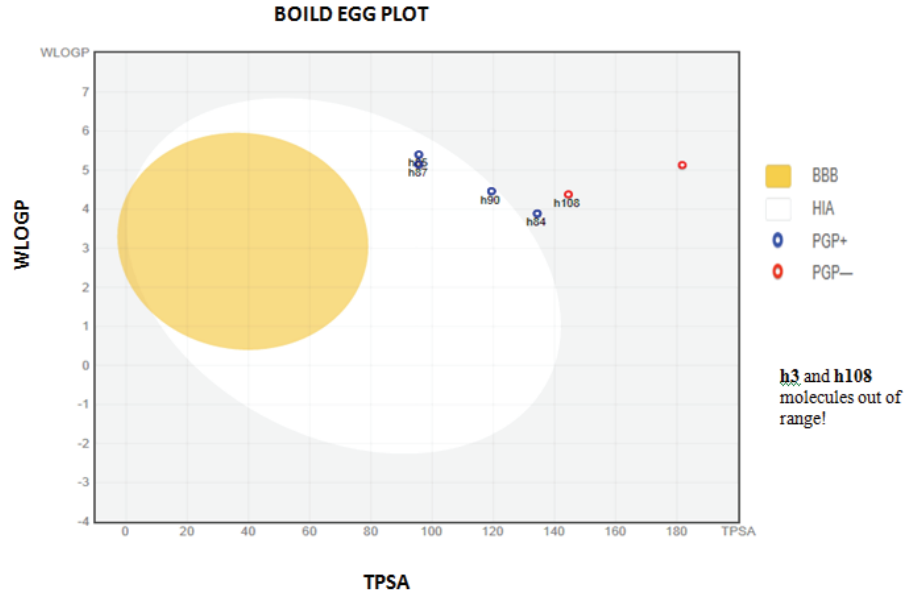

Fig 3. Boiled-Egg Plot.

The Pro-Tox online server provides predictions for four toxicity endpoints, which include hepatotoxicity, cytotoxicity, carcinogenicity, and mutagenicity. Additionally, it calculates an LD_{50} value for acute toxicity in rats (Table IV). Except for h85 and h87, which had positive predictions for cytotoxicity and carcinogenicity, the results demonstrated that all other compounds proved to be non--toxic. The results of LD_{50} of all compounds are presented in Table IV, and the value of h3, h84, h108 and h110is high, 1500–3000 mg/kg, which recommended that these compounds only have a lethal effect at high doses. Comparing that, the

three bioactive ligands h85, h87 and h90 with lower doses are more lethal than the compounds with higher LD_{50}.

Compounds h85 and h87 adhered to the rules with no more than one violation, displaying favorable ADMET proprieties. This suggests their potential as orally active lead molecules. Consequently, h85 and h87 were selected as models for MD investigation, specifically focusing on their stability within the Mpro binding site.[49]

Conformational dynamics and stability

We investigated the conformational stability, structural dynamics, and protein–ligand interactions of the h85 andh87 compounds and the 6LU7 receptor using 100 ns (MD simulation). The *RMSD* values for the two complexes started with a constant rise and are progressively equilibrating with just a slight variation, as expected. The *RMSD* for h85-6LU7 slightly deviates between 40 and 70 ns, then stays balanced and averages about 2.4 Å until the completion of the run (Fig. 4c). For the second complex h87-6LU7, the *RMSD* values of protein and

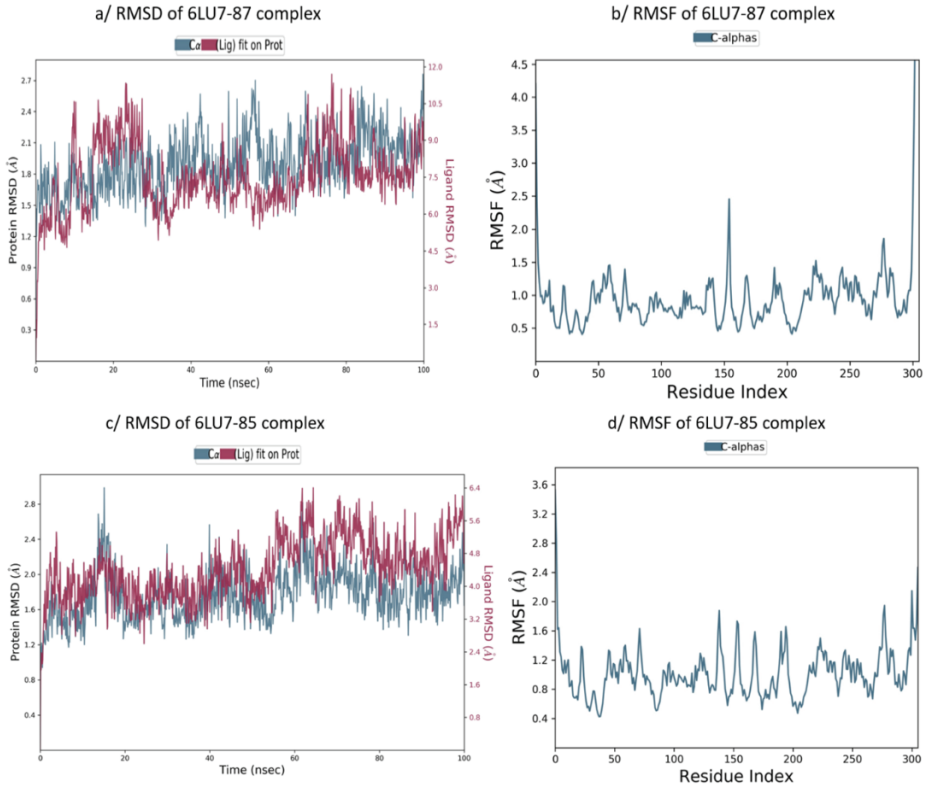

Fig 4. a) *RMSD* plot of 6LU7-h87 complex. b) *RMSF* plot of C-alpha atoms for 6LU7-h87. c) *RMSD* plot of 6LU7-h85 complex. d) *RMSF* plot of C-alpha atoms for 6LU7-h85.

ligand remain constant at around 2.4 Å (Fig. 4a). Both *RMSD*s exhibit minimal change after achieving equilibrium and both systems have C-alpha *RMSD*s less than 2.8 Å, suggesting that they are stable.

The study of the stability of complexes under consideration was further assessed by studying the evolution of their *RMSF*, as illustrated in Fig. 4b and d. The *RMSF* was used to measure each residue's flexibility capability and to investigate inhibitor binding to the target.[54] *RMSF* was performed on the protein backbone in this study, and it demonstrates a similar trend in both systems. The average *RMSF* values for h85-6LU7 and h87-6LU7 were 2.5 and 2, respectively. Furthermore, the residues 150 and 300 in h85-6LLU7 are very flexible, and the h87––6LU7 fluctuation arises at residues 140, 150–200 and 280–300. Moreover, the residues in the helix and loop (150–300) closest to the ligand show some fluctuation and flexibility. There is an h85-6LU7 flexible loop with a fluctuation greater than 4.5. Overall, the *RMSF* figure demonstrates that the binding of h85 and h87 to 6LU7 does not influence residual fluctuations, indicating that these complexes are adequately stable.

By observing the interaction histogram throughout the simulation duration (Fig. 5), there are at least three residues (GLU166, GLN189 and THR190) that

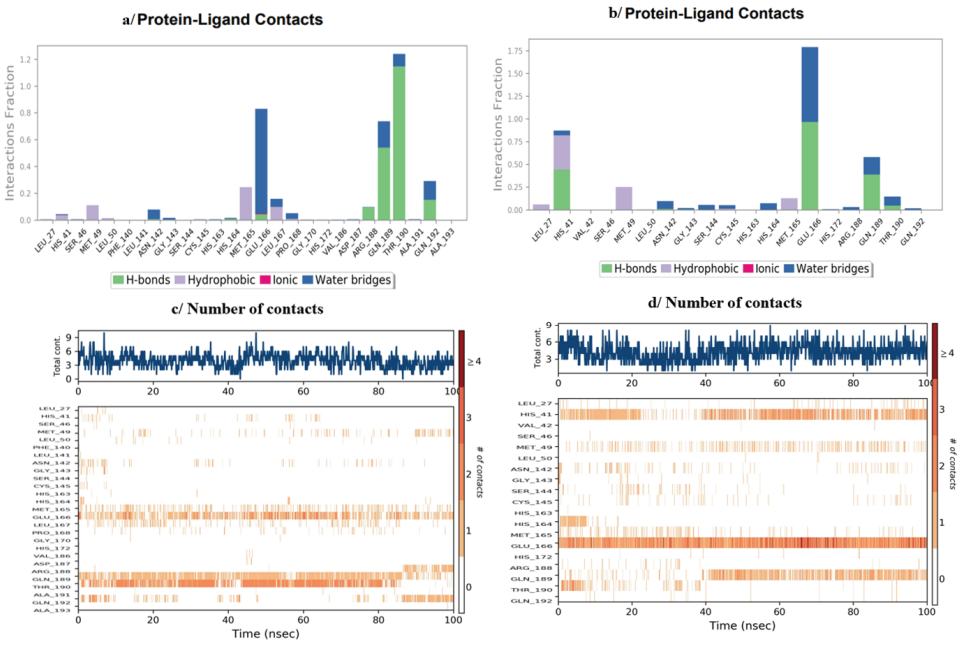

Fig. 5. MD simulations results of h85 and h87. a) The histogram of 6LU7-h85 interactions throughout the trajectory. b) The histogram of 6LU7-h87 interactions throughout the trajectory. c) Bar charts of 6LU7-h85 number of contacts. d) Bar charts of 6LU7-h85 number of contacts.

interact between ligand h85 and COVID-19 main protease for 100 ns either through hydrogen bonds, hydrophobic interactions or water bridges (Fig. 5a), which have the greatest number of contacts between 2 and 3 (Fig. 5c). While ligand h87 formed three important interactions with the main protease (HIS41, GLU166 and GLN189), including hydrogen bonds, water bridges and hydrophobic bridges (Fig. 5b), the number of contacts went from 2 to 3 (Fig. 5d).

CONCLUSION

The coronavirus pandemic, which has affected many countries and changed the rhythm of life during the years 2020–2022, is now a one of the main concern for the whole globe. In this study, we prepared 118 natural compounds and used advanced molecular docking and dynamic simulation to characterize and screen potential bioactive compounds against the coronavirus. Only 7 compounds demonstrated good binding affinity in comparison to the reference bioactive compound N3. The overall binding energies of the seven ligands except h110 ranged between –31.903 and –35.336 kJ/mol, which is similar to the energy value of the reference ligand N3 (–32.615 kJ/mol).

Based on the ADME analysis and molecular docking investigations, two specific ligands, h85 and h87, have shown potential as inhibitors of the coronavirus. This study serves as a preliminary selection to allow further experimental studies; by *in vitro* and *in vivo* methods to explore the pharmacokinetic aspects and adverse effects of these two compounds, for the design of possible future potential drugs against SARS-CoV-2.

SUPPLEMENTARY MATERIAL

Additional data and information are available electronically at the pages of journal website: https://www.shd-pub.org.rs/index.php/JSCS/article/view/12757, or from the corresponding author on request.

ИЗВОД

ИСТРАЖИВАЊЕ ЕФИКАСНОСТИ ПРИРОДНИХ ПРОИЗВОДА ПРЕМА SARS-COV-2: СИНЕРГИСТИЧКИ ПРИСТУП КОЈИ УКЉУЧУЈЕ СИМУЛАЦИЈЕ МОЛЕКУЛСКИМ ДОКИНГОМ И МОЛЕКУЛСКОМ ДИНАМИКОМ

NABILA AOUMEUR[1], MEBARKA OUASSAF[2], SALAH BELAIDI[2], NOUREDDINE TCHOUAR[1], LOFTI BOURAGAA[2], IMANE YAMARI[3], SAMIR CHTITA[3] и LEENA SINHA[4]

[1]University of Sciences and Technologies of Oran (USTO), Laboratory of Process Engineering and Environment, BP 1503 Oran 31000, Algeria, [2]Biskra University, LMCE Laboratory, Department of Matter Sciences, Biskra, Algeria, [3]Hassan II University of Casablanca, Laboratory of Analytical and Molecular Chemistry, Casablanca, Morocco и [4]University of Lucknow, Department of Physics, 226007 Lucknow, India

Главни циљ овог истраживања је да допринесе истраживању SARS-CoV-2 идентификацијом потенцијалних водећих једињења за клиничке примене, са посебним фокусом на инхибиторе који циљају главну протеазу (M^{pro}). У овом истраживању урађена је докинг анализа користећи софтвер *molecular operating environmental* (MOE) за процену потенцијала биоактивних једињења, добијених из лековитих биљака, као инхибитора

SARS-CoV-2 M^{pro}. Међу 118 природних производа са *anti*-HIV карактеристикама, седам најбољих кандидата (h3, h84, h85, h87, h90, h108 и h110), је идентификовано на основу бољих енергија везивања у поређењу са референтним лигандом N3. Ова одабрана једињења показују везивне афинитете од -33,996, −35,336, −32,615, −32,154, −33,452, −31,903, односно −40,360 kJ mol^{-1}. Да би даље сузили листу потенцијалних кандидата за примену код људи, испитали смо сличност са лековима, и фармацеутске атрибуте ових једињења користећи SwissADME мрежни сервер. Међу њима, само два једињења, наиме h85 и h87, су показала пожељне фармаколошке особине погодне за примену код људи. Ова два једињења су потом издвојена за даље испитивање. Да би истражили конформациону стабилност лиганада у M^{pro} активном месту, извели смо симулације молекулском динамиком (MD). Ове симулације су показале поуздане и постојане трајекторије, подржане анализом средњих квадратних флуктуација (*RMSF*) и средњих квадратних девијација (*RMSD*). Ови налази и пожељне молекулске особине и интеракциони профили сугеришу да ова два водећа једињења могу бити обећавајући SARS-CoV-2 терапијски кандидати. Она су узбудљиве полазне тачке за даљи дизајн лекова.

(Примљено 4. јануара, ревидирано 28. јануара, прихваћено 3. марта 2024)

REFERENCES

1. W. Guan, Z. Ni, Y. Hu, W. Liang, C. Ou, J. He, L. Liu, H. Shan, C. Lei, D. Hui, B. Du, L. Li, G. Zeng, K. Yuen, R. Chen, C. Tang, T. Wang, P. Chen, J. Xiang, S. Li, J. L. Wang, Z. Liang, Y. Peng, L. Wei, Y. Liu, Y. H. Hu, P. Peng, J. M. Wang, J. Liu, Z. Chen, G. Li, Z .Zheng, S. Qiu, J. Luo, C. Ye , S. Zhu, N. Zhong, *N. Eng. J. Med.* **382** (2020) 17085 (https://doi.org/10.1056/NEJMoa2002032)
2. C. Huang, Y. Wang, X. Li, L. Ren, J. Zhao, Y. Hu, L. Zhang, G. Fan, J. Xu, X. Gu, Z. Cheng, T. Yu, J. Xia, Y. Wei, W. Wu, X. Xie, W. Yin, H. Li, M. Liu, B. Cao, *Lancet* **395** (2020) 497 (https://doi.org/10.1016/S0140-6736(20)30183-5)
3. Y. C. Wu, C. S. Chen,Y. J. Chan. *J. Chinese Med. Assoc.* **83** (2020) 217 (https://doi.org/10.1097/JCMA.0000000000000270)
4. Z.Y.Zu, M. D. Jiang, P. P. Xu, W. Chen, Q. Q. Ni, G. M. Lu, L. J. Zhang, *Radiology* **296** (2020) E15 (https://doi.org/10.1148/radiol.2020200490)
5. A. A. T. Naqvi, K. Fatima, T. Mohammad, U. Fatima, I. K. Singh, A. Singh, S. M . Atif, G. Hariprasad, G. M. Hasan, M. I. Hassan, *Mol. Basis Dis*. **1866** (2020) 165878 (https://doi.org/10.1016/j.bbadis.2020.165878)
6. S.Mahmud, S.Biswas, G. Kumar Paul, A. M. Mita, S. Afrose, M. Robiul Hasan, M. Sharmin Sultana Shimu, M. A. R. Uddin, M. Salah Uddin, S. Zaman, K. M. Kaderi Kibria, M. Arif Khan, T. Bin Emran, M. Abu Saleh, *Arab. J. Chem*. **14** (2021) 103315 (https://doi.org/10.1016/j.arabjc.2021.103315)
7. N. Zhu, D. Zhang, W. Wang, X. Li, B. Yang, J. Song, X. Zhao, B. Huang, W. Shi, R. Lu, P. Niu, F. Zhan, X. Ma, D. Wang, W. Xu, G. Wu, G. F Gao, W.A. Tan, *N. Eng. J. Med.* **382** (2020) 727 (https://doi.org/10.1056/NEJMoa2001017)
8. X. Cui, Y. Wang, J. Zhai, M. Xue, C. Zheng, L. Yu, *Virus Research* **328** (2023) 199075 (https://doi.org/10.1016/j.virusres.2023.199075)
9. R. Gili, R. Burioni, *J. Transl. Med.* **21** (2023) 251(https://doi.org/10.1186/s12967-023-04095-6)
10. WHO world Health Organization [WHO], *Tracking SARS-CoV-2 variants*, 2023, https://www. who.int/activities/tracking-SARS-CoV-2-variants
11. W. T. Harvey, A. M. Carabelli, B. Jackson, R. K. Gupta, E. C. Thomson, E. M. Harrison, C. A. Ludden, R. Reeve, A. Rambaut, COVID-19 Genomics UK (COG-UK) Consortium,

S. J. Peacock, D. L. Robertson, *Nat. Rev. Microbiol.* **19** (2021) 409 (https://doi.org/10.1038/s41579-021-00573-0)
12. S. O. Aftab, M. Z. Ghouri, M. U. Masood, Z. Haider, Z. Khan, A. Ahmad, N. Munawar, *Transl. Med.* **18** (2020) 275(https://doi.org/10.1186/s12967-020-02439-0)
13. R. Yu, L. Chen, R. Lan, R. Shen, P. Li, *Int. J. Antimicrob. Agents* **56** (2020) 106012 (https://doi.org/10.1016/j.ijantimicag.2020.106012)
14. M. Lounasmaa, P. Hanhunen, M. Westersund, N. Halonen, *Alkaloids: Chem. Biol.* **52** (1999) 103(https://doi.org/10.1016/S0099-9598(08)60026-7)
15. R. M. Perez, *Pharm. Biol.* **41** (2003) 107 (https://doi.org/10.1076/phbi.41.2.107.14240)
16. S. Chtita, R. T. Fouedjou, S. Belaidi, L. A. Djoumbissie, M. Ouassaf, F. A. Qais, M Bakhouch, M. Efendi, T. T. Tok, M. Bouachrine, T. Lakhlifi, *Struct Chem*. **33** (2022) 1799 (https://doi.org/10.1007/s11224-022-01939-7)
17. J. G. Africa, H. C. Arturo, L. J. Bernardo, J. K. Ching, O. C. de la Cruz, J. B. Hernandez, R. J. Magsipoc, C. T. Sales, J. C. Agbay, G. L. Neri, M. T. Quimque, A. P. Macabeo, *Philipp. J. Sci*. **151** (2021) 35 (https://doi.org/10.56899/151.01.04)
18. P. Gale, *Micro. Risk. Anal*. **21** (2022)100198 (https://doi.org/10.1016/j.mran.2021.100198)
19. P. Gale, *Micro. Risk. Anal*. **16** (2020) 100140 (https://doi.org/10.1016/j.mran.2020.100140)
20. M. Popovic, *Micro. Risk. Anal*. **23** (2023) 100250 (https://doi.org/10.1016/j.mran.2023.100250)
21. M. Popovic and M. Popovic, *Micro. Risk. Anal*. **21** (2022)100202 (https://doi.org/10.1016/j.mran.2022.100202)
22. M. Popovic, *Micro.Risk.Anal*.**24** (2023) 100260 (https://doi.org/10.1016/j.mran.2023.100260)
23. M. E. Popovic, M. P. Pavlovic, M. Papovic, *Micro. Risk. Anal*. **25** (2023) 100280
24. (https://doi.org/10.1016/j.mran.2023.100280)
25. B. Hemmateenejad, K. Javidnia, M. Nematollahi, M. Elyasi, *J. Iran. Chem. Soc.* **6** (2009) 420 (https://doi.org/10.1007/BF03245853)
26. A. Aouidate, A. Ghaleb, S. Chtita, M. Aarjane, A. Ousaa, H. Maghat, A. Sbai, M. Choukrad, M. Bouachrine, T. Lakhlifi, *J. Biomol. Struct. Dyn*. **39** (2021)4522 (https://doi.org/10.1080/07391102.2020.1779130)
27. R. Banerjee, L. Perera, L. M. V. Tillekeratne, *Drug .Discov. Today* **26** (2021) 804 (https://doi.org/10.1016/j.drudis.2020.12.005)
28. P. K. Doharey, V. Singh, M. R. Gedda, A. K. Sahoo, P. K. Varadwaj, B. Sharma, *J. Biomol. Struct. Dyn.* **40** (2022) 5588 (https://doi.org/10.1080/07391102.2021.1871956)
29. M. T. J. Quimque, K. I. R. Notarte, R. A. T. Fernandez, M. A. O. Mendoza, R. A. D. Liman, J. A. K. Lim, L. A. E. Pilapil, J. K. H. Ong, A. M. Pastrana, A. Khan, D. Q. Wei, A. P. G. Macabeo, *J. Biomol. Struct. Dyn.* **39** (2021) 4316 (https://doi.org/10.1080/07391102.2020.1776639)
30. V. N. O. de Leon, J. A. H. Manzano, D. Y. H. Pilapil, R. A. T. Fernandez, J. K. A. R. Ching, M. T. J. Quimque, J.C.M. Agbay, K. I. R. Notarte, A. P. G. Macabeo, *J. Genet. Eng. Biotechnol*. **19** (2021) 104 (https://doi.org/10.1186/s43141-021-00206-2)
31. D. Li, J. Luan, L. Zhang, *Biochem. Biophys. Res. Commun.* **538** (2021) 72 (https://doi.org/10.1016/j.bbrc.2020.11.083)
32. HYPERCHEM Molecular Modeling System, Hypercube. Inc., Gainesville, FL, 2007
33. MARVINSKETCH 17.1.2, ChemAxon 2017 (http://www.chemaxon.com)

34. S. Belaidi, R. Mazri, H. Belaidi, T. Lanez, D. Bouzidi, *Asian J. Chem*. **25** (2013) 9241 (https://doi.org/10.14233/ajchem.2013.15199)
35. A. Kerassa, S. Belaidi, D. Harkati, T. Lanez, O. Prasad, L. Sinha, *Rev. Theor. Sci.* **4** (2016) 85 (https://doi.org/10.1166/rits.2016.1050)
36. S. Chtita, A.Belhassan, A. Aouidate, S. Belaidi, M. Bouachrine, T. Lakhlifi, *Comb. Chem. High Throughput Screen*. **24** (2021) 441 (https://doi.org/10.2174/1386207323999200730205447)
37. Molecular Operating Environment (MOE), Version 2007.09, Chemical Computing Group, Inc., Montreal, Quebec, 2005 (http://www.Chemcomp.com)
38. P. S. Das, A. Kokardekar, C. M. Breneman, *J. Chem. Inf. Model*. **49** (2009) 2863 (https://doi.org/10.1021/ci900317x)
39. M. Ouassaf, S. Belaidi, S. Khamouli, H. Belaid, S. Chtita, *Acta Chim. Slov.* **68** (2021) 289 (https://doi.org/10.17344/acsi.2020.5985)
40. C. A. Lipinski, F. Lombardo, B. W. Dominy, P. J. Feeney, *Adv. Drug. Deliv. Rev.* **46** (2001) 3 (https://doi.org/10.1016/s0169-409x(00)00129-0)
41. A. Daina, O. Michielin, V. Zoete, *Sci. Rep.* **7** (2017) 42717 (https://doi.org/10.1038/srep42717)
42. Schrödinger Release 2021-3: Maestro-Desmond Interoperability Tools, Schrödinger, LLC, New York
43. K. Roos, C. Wu, W. Damm, M. RebouL, J. M. Stevenson, C. Lu, M. K. Dahlgren, S. Mondal, W. Chen, L. Wang, R. Abel, R. A. Friesner, E. D. Harder, *J. Chem. Theory Comput.* **15** (2019) 1863(https://doi.org/10.1021/acs.jctc.8b01026)
44. A. Imberty, C. Gautier, J. Lescar, S. Pérez, L. Wyns, R. Loris, *J. Biol. Chem.* **275** (2000) 17541 (https://doi.org/10.1074/jbc.M000560200)
45. K. O. Chang, Y. Kim, S. Lovell, A. D. Rathnayake, W. C. Groutas, *Viruses* **11** (2019) 197 (https://doi.org/10.3390/v11020197)
46. D. F. Veber, S. R. Johnson, H. Y. Cheng, B. R. Smith, K. W. Ward, K. D. Kopple, *J. Med. Chem.* **45** (2002) 2615 (https://doi.org/10.1021/jm020017n)
47. A. K. Ghose, V. N. Viswanadhan, J. J. Wendoloski, *J. Comb. Chem.* **1** (1999) 55 (https://doi.org/10.1021/cc9800071)
48. I. Muegge, S. L. Heald, D. Brittelli, *J. Med. Chem.* **44** (2001) 1841 (https://doi.org/10.1021/jm015507e)
49. W. J. Egan, K. M. Merz, J. J. Baldwin, *J. Med. Chem*. **43** (2000) 3867 (https://doi.org/10.1021/jm000292e)
50. A. Zerroug , S. Belaidi, I. BenBrahim, L. Sinha, S. Chtita, *J. King Saud Univ. Sci*. **31** (2019) 595-560 (https://doi.org/10.1016/j.jksus.2018.03.024)
51. N. Aoumeur, S. Belaidi, N. Tchouar, M. Ouassaf, T. Lanez, S. Chtita, *Mor. J. Chem.* **9** (2021) 274 (https://doi.org/10.48317/IMIST.PRSM/morjchem-v9i2.19884)
52. H. Nour, O. Daoui, O. Abchir, S. ElKhattabi, S. Belaidi, S. Chtita, *Heliyon* **8** (2022) e11991 (https://doi.org/10.1016/j.heliyon.2022.e11991)
53. A. Daina, V. Zoete, *J. Med. Chem.* **6** (2016) 1117 (https://doi.org/10.1002/cmdc.201600182)
54. V. Zoete, A. Daina, C. Bovigny, O. Michielin, *J. Chem. Info. Model.* **56** (2016) 1399 (https://doi.org/10.1021/acs.jcim.6b00174)
55. S. Ghahremanian, M. M. Rashidi, K. Raeisi, D. Toghraie. *J. Mol. Liq*. **354** (2022) 118901 (https://doi.org/10.1016/j.molliq.2022.118901).